FLIGHT RESULTS FOR A REVOLUTIONARY APPROACH TO MAXIMIZING SPACECRAFT IMAGING CAPABILITY

Mark Karpenko(1)**, Sagar Bhatt**(2)**, Nazareth Bedrossian**(2)**, and I. Michael Ross**(1)
(1)*Naval Postgraduate School, Monterey, CA 93943.*
(2)*The Charles Stark Draper Laboratory, Houston, TX, 77058.*

Abstract: *This paper presents the design and flight implementation of shortest-time maneuvers on the TRACE spacecraft. Shortest-time maneuvers (STM)s are spacecraft slew maneuvers, based on optimal control theory, that enable spacecraft to be maneuvered more quickly than conventional rotations. The STMs are obtained by constructing a minimum-time optimal control problem formulation that can be rapidly solved using pseudospectral optimal control theory. To ensure each STM trajectory is well within the capabilities of the spacecraft, the formulation of the optimal control problem includes all of the relevant nonlinear dynamics of the reaction wheel satellite as well as appropriate state and control constraints, such as the nonlinear actuator torque-momentum envelope. Flight test results for several maneuvers, all relevant to the operation of a typical Earth imaging satellite, are presented in order to illustrate various aspects of the revolutionary STM capability. The flight results demonstrate that STMs can not only be implemented and reliably executed on orbit, but that implementing STMs enables spacecraft imaging capability to be improved simply by changing the commanded maneuver trajectories. Moreover, it is possible to implement the idea without the need to modify the spacecraft attitude control system. This feature allows the capabilities of existing Earth imaging and related spacecraft to be extended beyond their original specifications in order to maximize mission performance.*

Keywords: *Minimum-time reorientation maneuvers, pseudospectral optimal control, flight experiments, attitude dynamics and control, spacecraft maneuver design and optimization.*

1. Introduction

Commercial Earth imaging satellites are used to acquire photographs and other specialized images of specific areas of the earth using their onboard sensors. Since each acquired image equates to a certain amount of revenue generation by the vehicle, there has been great interest in developing algorithms for managing the profitability of imaging satellites (see, for example, [1, 2] and the references therein). The main problem addressed in this paper is how to execute the sequence of image acquisitions that best utilizes the capabilities of the vehicle, while maximizing revenue.

A significant factor impacting the maneuver planning process is the amount of time that is needed to slew the spacecraft between the possible image collection regions since there exists only a finite time during which each region of interest is in the field of view of the imagining sensors. Thus, the ability to transition between each imaging region as quickly as possible reduces "waste time" [3] and increases the number of images that can be acquired during a given window. Because slew time has a direct influence on the productivity of imaging satellites as well as other scientific missions, time-optimal attitude maneuvers have been the subject of extensive study in the literature [4–10]. The main discovery arising from this research is the fact that conventional eigenaxis rotations, which give the shortest angular path between two orientations, are slower than minimum-time maneuvers. This is because the axis of rotation is restricted to the eigenaxis, which inherently limits the maximum spacecraft rotation rate. Time-optimal attitude maneuvering, on the other hand, requires a careful choreography that synchronizes simultaneous rotations of the spacecraft around all three axes of the body-fixed frame. By rotating about all axes simultaneously, the spacecraft rotation rate can be increased far beyond the eigenaxis limit. The resulting shortest-time attitude trajectory allows the spacecraft to be reoriented more quickly than by following the eigenaxis path.

The objective of this paper is to present results, relevant to the operation of Earth imaging satellites, obtained from the first ever flight demonstration of time-optimal maneuvering [11]. These shortest-time maneuvers (STMs) are based on optimal control theory and were implemented onboard the NASA Transition Region and Coronal Explorer (TRACE). In this paper, a variety of operationally relevant STMs are presented that demonstrate rapid maneuvering capability on a real satellite with a reaction wheel attitude control system. In order to design STMs for this practical space system, the underlying optimal control problem had to include all of the relevant nonlinear spacecraft dynamics as well as complex state and control constraints, for example, the nonlinear reaction wheel torque-momentum envelope. The STMs were solved using pseudospectral (PS) optimal control theory [12–14] implemented in the optimal control software DIDO [15]. The TRACE flight demonstration is the second time PS optimal control theory has been used by NASA on orbit. In fact, PS optimal control theory debuted in flight on November 5, 2006 when NASA used it to implement Bedrossian's zero-propellant (fuel-optimal) maneuver onboard the International Space Station [16].

Several flight test results are presented to illustrate how the STM paradigm has the potential to maximize spacecraft imaging capability. Although TRACE is a Sun pointing satellite rather than an Earth pointing system, the maneuver scenarios performed onboard TRACE were designed to closely emulate various activities that are relevant to imaging operations on an Earth imaging satellite. In one experiment, a sequence of STMs that minimize the time to slew through a sorted set of static imaging points demonstrates how STMs can be used to improve data collection throughput within a given imaging window. The results of a second experiment involving an emulated scanning operation demonstrates how STMs can be utilized to quickly transition the spacecraft between point collection and scanning tasks.

The successful implementation of these maneuvers illustrate that the STM paradigm can be reliably executed on orbit and can significantly improve the agility of the spacecraft as compared to standard techniques. Moreover, the performance improvement can be realized through a simple change in the commanded maneuver trajectories and without the need to perform costly modifications on the existing spacecraft attitude control system. Thus, it is now possible to insert the revolutionary approach for maximizing spacecraft imaging capability into normal mission operations and extend the capabilities of existing Earth imaging satellites beyond their original design specifications.

2. The TRACE Spacecraft

2.1. Equations of Motion

Fig. 1 shows a photograph of the Transition Region and Coronal Explorer (TRACE) undergoing a pre-launch checkout at NASA. TRACE is a reaction wheel spacecraft designed to perform small angle slews, less than 1 deg, in order to document the fine scale magnetic features of the solar surface and corona [17]. Although not part of the original mission objectives, the spacecraft is capable of executing large angle eigenaxis maneuvers by using a nonlinear momentum control logic that is implemented as part of the flight software.

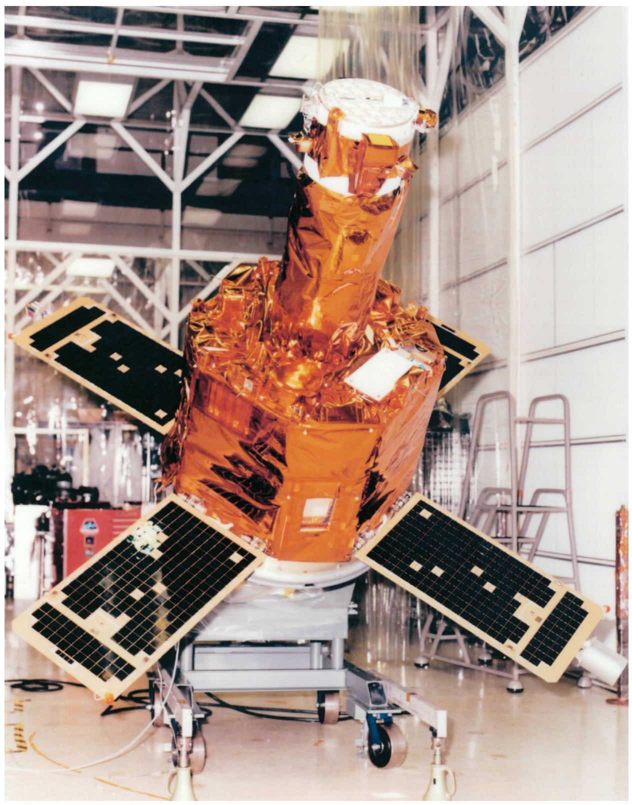

Figure 1. TRACE undergoing a pre-launch checkout at NASA.

The rotational dynamics of the TRACE satellite can be derived by considering the angular momentum of the reaction wheel satellite system

$$\mathbf{H} = \mathbf{I}\omega + \sum_{i=1}^{4} \mathbf{a}_i h_{\mathrm{w},i} \tag{1}$$

where $\mathbf{H}$ is the total angular momentum of the system with respect to the body-fixed frame. Matrix $\mathbf{I}$ is the inertia tensor of the spacecraft with freely rotating reaction wheels, and vector ω is the angular rate of the spacecraft expressed in the body frame. Unit vectors $\mathbf{a}_i$ give the orientation of the spin axis of each reaction wheel with respect to the spacecraft coordinate system. Each product, $\mathbf{a}_i h_{\mathrm{w},i}$, represents the transformation of the reaction wheel momentum from the actuator frame to the body-fixed frame.

In the absence of any external torques acting on the spacecraft, the time rate of change of the angular momentum in the inertial frame is

$$\frac{\mathrm{d}}{\mathrm{dt}}(\mathbf{H}) + \omega \times \mathbf{H} = 0 \tag{2}$$

Equation (2) can be expanded and rearranged to give Euler's equation

$$\mathbf{I}\dot{\omega} + \sum_{i=1}^{4} \mathbf{a}_i \dot{h}_{\mathrm{w},i} + \omega \times (\mathbf{I}\omega + \sum_{i=1}^{4} \mathbf{a}_i h_{\mathrm{w},i}) = 0 \tag{3}$$

The angular momentum of each reaction wheel about its axis of rotation is

$$h_{\mathrm{w},i} = I_{\mathrm{w},i}(\Omega_{\mathrm{w},i} + \mathbf{a}_i^T \omega) \tag{4}$$

where $I_{\mathrm{w},i}$ is the inertia of the reaction wheel about its spin axis, and $\Omega_{\mathrm{w},i}$ is the angular rate of the reaction wheel relative to the satellite body. The rate of change of the reaction wheel momentum is directly proportional to the torque, $\tau_{\mathrm{w},i} = \dot{h}_{\mathrm{w},i}$, applied around the spin axis by the reaction wheel speed control system. Thus, the equation describing the reaction wheel dynamics is obtained simply, by differentiating (4).

Using (3) together with (4) and its derivative, the spacecraft rotational dynamics can be written in the following matrix form

$$\Gamma \begin{bmatrix} \dot{\omega} \\ \dot{\Omega}_{\mathrm{w},1} \\ \vdots \\ \dot{\Omega}_{\mathrm{w},4} \end{bmatrix} = \begin{bmatrix} -\omega \times \left(\mathbf{I}\omega + \sum_{i=1}^{4} \mathbf{a}_i I_{\mathrm{w},i} \omega_{\mathrm{w},i} + \mathbf{a}_i I_{\mathrm{w},i} \mathbf{a}_i^T \omega \right) \\ \tau_{\mathrm{w},1} \\ \vdots \\ \tau_{\mathrm{w},4} \end{bmatrix} \tag{5}$$

where

$$\Gamma = \begin{bmatrix} \mathbf{I} + \sum_{i=1}^{4} \mathbf{a}_i I_{\mathrm{w},i} \mathbf{a}_i^T & \mathbf{a}_1 I_{\mathrm{w},1} & \cdots & \mathbf{a}_4 I_{\mathrm{w},4} \\ I_{\mathrm{w},1}\mathbf{a}_1^T & I_{\mathrm{w},1} & \cdots & 0 \\ \vdots & \vdots & \ddots & \vdots \\ I_{\mathrm{w},4}\mathbf{a}_4^T & 0 & \cdots & I_{\mathrm{w},4} \end{bmatrix} \tag{6}$$

To complete the mathematical model of the spacecraft dynamics, the attitude of the spacecraft is described using quaternions parameterized as

$$\mathbf{q} = \left[e_1 \sin\left(\tfrac{\Phi}{2}\right), e_2 \sin\left(\tfrac{\Phi}{2}\right), e_3 \sin\left(\tfrac{\Phi}{2}\right), \cos\left(\tfrac{\Phi}{2}\right) \right]^T \tag{7}$$

where $\mathbf{e} = [e_1, e_2, e_3]$ is the Euler vector (eigenaxis) and Φ is the rotation angle around the eigenaxis. The corresponding quaternion differential equation is [18]

$$\dot{\mathbf{q}} = \tfrac{1}{2}\mathbf{Q}(\omega)\mathbf{q} \tag{8}$$

where the skew-symmetric matrix $\mathbf{Q}(\omega)$ is given as

$$\mathbf{Q}(\omega) = \begin{bmatrix} 0 & \omega_3 & -\omega_2 & \omega_1 \\ -\omega_3 & 0 & \omega_1 & \omega_2 \\ \omega_2 & -\omega_1 & 0 & \omega_3 \\ -\omega_1 & -\omega_2 & -\omega_3 & 0 \end{bmatrix} \tag{9}$$

2.2. Attitude Control System

The TRACE spacecraft employs four reaction wheels arranged in a tetrahedral array for primary attitude control. This arrangement gives four for three redundancy and ensures that full control capability is retained in the event of a failure of any single wheel [19]. The spacecraft body rates are measured using three dual-axis gyros. On board quaternion propagation is carried using the rate gyros in conjunction with measurements from a three-axis fluxgate magnetometer and a Kalman filter.

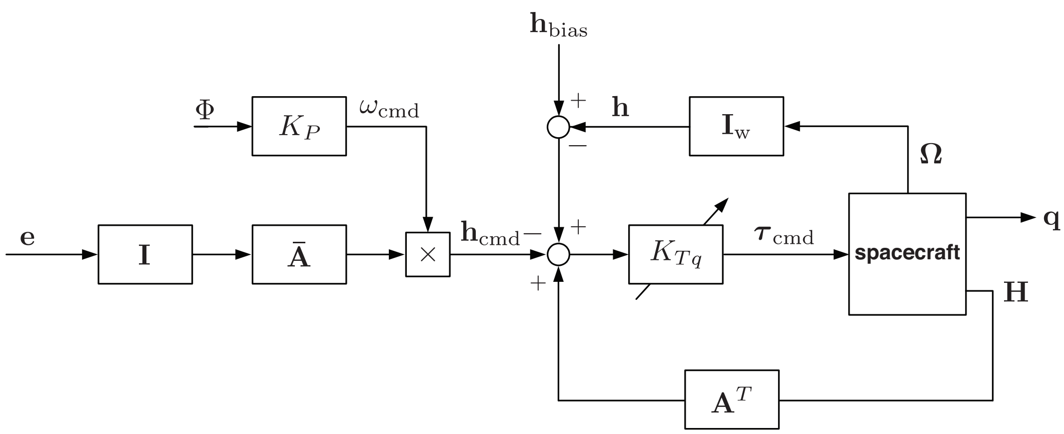

Figure 2. Block diagram of TRACE attitude control system.

A block diagram of the TRACE ACS is shown in Fig. 2. Since the ACS was originally designed to implement eigenaxis maneuvers, the first step in the control process is to determine the rotation angle, Φ, and Euler axis, $\mathbf{e}$, that zeros the attitude error with respect to the current target quaternion. The control logic then determines an appropriate spacecraft rate command, depending on the magnitude of the computed rotation angle. In the flight experiments presented in this paper, the rate command is proportional to the desired rotation angle

$$\omega_{\text{cmd}} = K_p \Phi \tag{10}$$

The reaction wheel momentum command vector, $\mathbf{h}_{\text{cmd}}$, is computed by distributing the rate command computed from (10) along the eigenaxis and accounting for the spacecraft inertia to obtain the commanded momentum in the spacecraft body frame. The momentum command is then transformed to the individual reaction wheel frames by control allocation matrix, $\bar{\mathbf{A}}$. The reaction wheel momentum command vector is (see Fig. 2)

$$\mathbf{h}_{\text{cmd}} = \omega_{\text{cmd}} \bar{\mathbf{A}} \mathbf{I} \mathbf{e} \tag{11}$$

The individual reaction wheel torques are then computed as

$$\tau_{\mathrm{cmd}} = K_{Tq}\left(\mathbf{h}_{\mathrm{cmd}} + \mathbf{A}^T\mathbf{H} + \mathbf{h}_{\mathrm{bias}} - \mathbf{h}\right) \tag{12}$$

where parameter K_{Tq} is an adjustable slew motor torque gain that is varied in order to enforce constraints on the maximum reaction wheel speed and power consumption. In (12), $\mathbf{A} = [\mathbf{a}_1|\mathbf{a}_2|\mathbf{a}_3|\mathbf{a}_4]$ is the column matrix of unit vectors relating the wheel spin axes to the spacecraft frame.

Prior to applying the commanded toques to the reaction wheel array, they are filtered in order to suppress excitation of the flexible modes inherent to the spacecraft structure. The torque command filters can be written in the following linear time-invariant form

$$\begin{aligned} \dot{\mathbf{x}}_{\mathrm{f}} &= \mathbf{A}_{\mathrm{f}}\mathbf{x}_{\mathrm{f}} + \mathbf{B}_{\mathrm{f}}\tau_{\mathrm{cmd},i} \\ \tau_{\mathrm{w},i} &= \mathbf{C}_{\mathrm{f}}\mathbf{x}_{\mathrm{f}} + \mathbf{D}_{\mathrm{f}}\tau_{\mathrm{cmd},i} \end{aligned} \tag{13}$$

where $\mathbf{x}_{\mathrm{f}}$ is the vector of filter states and $\mathbf{A}_{\mathrm{f}}$, $\mathbf{B}_{\mathrm{f}}$, $\mathbf{C}_{\mathrm{f}}$, and $\mathbf{D}_{\mathrm{f}}$ are the matrices of filter coefficients with the appropriate dimensions.

3. Maximizing Attitude Control Capability

3.1. Spacecraft Agilitoid

The attitude control capability of a spacecraft can be visualized in terms of an "agilitoid" [14]. This agilitoid is generated by mapping the available momentum-to-inertia ratio,

$$A(\xi) = \frac{h(\xi)}{I_\xi} \tag{14}$$

over a 2π steradian, where $h(\xi)$ is the angular momentum of the spacecraft about an arbitrary axis, ξ, and I_ξ is the moment of inertia of the spacecraft along ξ. The agilitoid for the TRACE spacecraft is shown in Fig. 3. The agilitoid (Fig. 3a) shows that the attitude control capability of TRACE is highly non-uniform. This is a direct result of how the reaction wheel configuration interacts with the spacecraft inertia ellipsoid. It is observed that the attitude control capability is largest around the s_2 (boresight) axis but is much smaller about the s_1 and s_3 axes. In fact, given the momentum capacity of the reaction wheel array, it is theoretically possible to rotate the TRACE spacecraft by more than 10-deg/sec about the boresight axis. In contrast, the maximum rotation rate about the other body axes is approximately 60% of this value. Thus, the agility of the spacecraft can be significantly improved by developing new, counterintuitive, reorientation maneuvers that can exploit the nonspherical geometry of the agilitoid. Such maneuvers would tend to deviate from the eigenaxis in favor of rotation about the boresight axis as a means of reducing the overall reorientation time. The approach for designing these new maneuvers is to formulate this shortest-time maneuver paradigm in terms of an optimal control problem.

Practical operation of the TRACE spacecraft is, however, severely limited by the per-axis software saturation limit of the onboard rate gyros ($\omega_{\mathrm{sat}} = 0.5$ deg/sec). The gyro saturation limits impose a restricted operating envelope in the momentum space which is significantly smaller than the capability of the reaction wheel array. This restricted operating envelope is shown in comparison with the agilitoid in Fig. 3b. The small size of the restricted operating envelope in conjunction with the fact that the per axis spacecraft rotation rates are all limited to the same value seems to imply that there is no real advantage to be gained by implementing shortest-time maneuvers in lieu of conventional eigenaxis slews. This argument would indeed be true if the restricted operating envelope were a sphere instead of a cube since for a sphere, $\omega_{\text{max}} = \omega_{\text{sat}}$ in any direction of rotation. For a cube shaped operating envelope, however, a rotation rate of $\omega_{\text{max}} = \sqrt{3}\omega_{\text{sat}}$ can be developed about each of the cube diagonals. Shortest-time maneuvers will exploit this fact to reduce the reorientation time between any two attitudes.

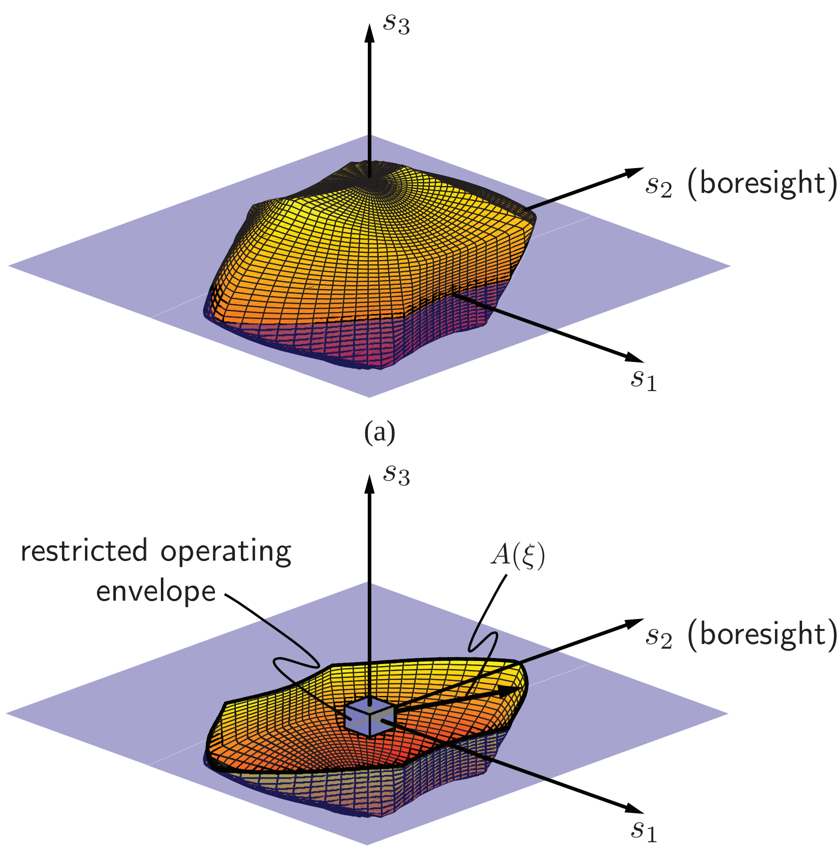

(b)

Figure 3. Attitude control capability of TRACE: (a) spacecraft agilitoid; (b) cutaway illustrating a value of $A(\xi)$ in the $s_1 - s_2$ plane and the restricted region of operation arising due to gyro saturation limits.

3.2. Optimal Control Formulation

An optimal control problem formulation was developed to design a variety of different STMs for the TRACE spacecraft. To ensure that the maneuvers could be reliably executed on the orbiting spacecraft, the minimum-time optimal control problem formulation incorporates all of the relevant spacecraft actuator and sensor constraints in addition to a detailed description of the spacecraft dynamics. The optimal control problem formulation is hereafter referred to as Problem B and has the following formulation

$$
\text{B:}\left\{
\begin{array}{lrl}
\text{Minimize} & J & = t_f \\
\text{Subject to} & \dot{\mathbf{x}}(t) & = \left\{ \begin{array}{l} \frac{1}{2}\mathbf{Q}(\omega_{\rm B})\mathbf{q} \\ \Gamma^{-1}\left[\begin{array}{c} -\omega_{\rm B} \times \left(\mathbf{J}\omega_{\rm B} + \sum_{i=1}^{4} \mathbf{a}_i I_{{\rm w},i}\omega_{{\rm w},i} + \mathbf{a}_i I_{{\rm w},i}\mathbf{a}_i^T \omega_{\rm B} \right) \\ \mathbf{C}_{\rm f}\mathbf{x}_{\rm f} + \mathbf{D}_{\rm f}\tau_{\rm cmd} \end{array} \right] \\ \mathbf{A}_{\rm f}\mathbf{x}_{\rm f} + \mathbf{B}_{\rm f}\tau_{\rm cmd} \end{array} \right\} \\
 & \mathbf{x}(t_0) & = \left[\mathbf{e}_0 \sin(\frac{\phi_0}{2}), \cos(\frac{\phi_0}{2}), \omega_0, \Omega_0, \mathbf{x}_{{\rm f},0}\right]^T \\
 & \mathbf{x}(t_f) & = \left[\mathbf{e}_f \sin(\frac{\phi_f}{2}), \cos(\frac{\phi_f}{2}), \omega_f, \Omega_f, \mathbf{x}_{{\rm f},f}\right]^T \\
 & ||\mathbf{q}(t)|| & = 1 \\
 & |\omega_i(t)| & \leq \omega_{\rm max}, \quad i = 1, \ldots, 3 \\
 & |\tau_{{\rm cmd},i}(t)| & \leq \tau_{\rm cmd,max}, \quad i = 1, \ldots, 4 \\
 & |I_{{\rm w},i}\Omega_{{\rm w},i}(t)| & \leq I_{{\rm w},i}\Omega_{\rm max}, \quad i = 1, \ldots, 4 \\
 & \tau_L & \leq I_{{\rm w},i}\dot{\Omega}_{{\rm w},i}(t) \leq \tau^U, \quad i = 1, \ldots, 4
\end{array}
\right. \tag{15}
$$

The solution to Problem B gives the state-control function pair, $t \to (\mathbf{x}, \tau_{\rm cmd})$, that drives the spacecraft from its initial orientation, $\mathbf{q}_0 = [\mathbf{e}_0 \sin(\frac{\Phi_0}{2}),\ \cos(\frac{\Phi_0}{2})]^T$, to the desired final attitude, $\mathbf{q}_f = [\mathbf{e}_f \sin(\frac{\Phi_f}{2}),\ \cos(\frac{\Phi_f}{2})]^T$, in the shortest time. In general, the resulting spacecraft attitude trajectories between any two desired orientations will deviate significantly from the smallest-angle (eigenaxis) trajectory between the same points.

In Problem B, the state space model of the spacecraft dynamics includes the dynamics of the reaction wheel torque command filters (13), as well as constraints on the commandable reaction wheel torque and limits on the reaction wheel momentum. Nonlinear reaction wheel power limits are incorporated by using the constraint, $\tau_L \leq I_{{\rm w},i}\dot{\Omega}_{{\rm w},i}(t) \leq \tau^U$, to ensure that the commanded torques always remain within the reaction wheel torque-momentum envelope. The absolute values of the spacecraft body rates also have to be constrained to avoid hard saturation of the rate gyros, a condition that would cause loss of control of the spacecraft. To ensure the spacecraft body rates always remain within the restricted operating envelope (see Fig. 3b), a software imposed rate limit was incorporated into the STM design.

Obtaining a solution to the optimal control problem (15) is challenging for several reasons including the high-dimensionality of the state space model (19 states and 4 controls), the nonlinear characteristics of the quaternion dynamics, the coupled nature of Euler's equations, and the need to consider both linear and nonlinear state and control constraints. Furthermore, a purported solution to the problem must be shown to satisfy the necessary conditions of optimality, which assert the existence of covector functions, $t \to (\lambda, \mu, \nu)$ that satisfy certain conditions with respect to the Lagrangian of the Hamiltonian, the endpoint Lagrangian, as well as complementarity conditions on the endpoint and path constraints [20]. The resulting "dualized" problem is a boundary value problem of 38 differential equations with both differential and algebraic constraints. Despite these traditional difficulties, it is possible to obtain solutions to problem (15) in a relatively straightforward fashion using PS optimal control theory.

3.3. Pseudospectral Optimal Control

In simple terms, PS optimal control theory is founded on expressing the state trajectory, $x(\cdot)$ as an infinite series expansion,

$$x(t) = \sum_{j=0}^{\infty} a_j P_j(t) \tag{16}$$

where $P_j(t)$ is a polynomial of degree, j. If $P_j(t)$ is chosen to be a Legendre polynomial of degree j, then it is called a Legendre PS method. Similarly, if $P_j(t)$ is chosen to be the $j-th$ degree Chebyshev polynomial, then it is called a Chebyshev PS method. The most common choices in PS optimal control theory are the Legendre and Chebyshev polynomials, although other polynomial basis functions may be used [21].

The coefficients a_j in (16) are called the spectral coefficients [13]. A key principle in a PS approach is that the spectral coefficients are computed "indirectly" by transforming (16) to the space of Lagrange interpolating polynomials. Thus, (16) is written equivalently as

$$x(t) = \sum_{j=0}^{\infty} \frac{W(t)}{W(t_j)} \phi_j(t) x_j \tag{17}$$

where $t_j,\ j = 0, 1, 2, \ldots$ are discrete points in time associated with a specific choice of $P_j(t), W(t)$ is a weight function that is also associated with $P_j(t)$ and $\phi_j(t)$ is a Lagrange interpolating polynomial that satisfies the Kronecker relationship

$$\phi_j(t_k) = \delta_{jk} \tag{18}$$

This property implies that

$$\begin{aligned} x(t_k) &= \sum_{j=0}^{\infty} \frac{W(t_k)}{W(t_j)} \phi_j(t_k) x_j \\ &= x_k \end{aligned} \tag{19}$$

It is this "sampling" property, which is absent in (16), that makes the PS approach distinct from the direct use of (16). Equation (19) illustrates that the global information in (17) is used to examine the local information at $t = t_k$. This is in sharp contrast to a Taylor series expansion,

$$x(t) = \sum_{j=0}^{\infty} \frac{t^j}{j!} x^{(j)}(0) \tag{20}$$

which uses local information (at $t = 0$) to construct global phenomenon. Because optimal control problems are fundamentally global (i.e. conditions at the final point affects the action taken at the initial point), it can be argued that (17) is a more natural fit than (20) for solving solving optimal control problems.

In practice, (17) cannot be implemented due to infinite summation (the same is true of 16 and 20). The best one can expect to achieve is a solution up to machine precision, $\varepsilon_m > 0$. In a series of theorems promulgated by Ross, Fahroo, Gong and Kang [12, 14, 22–27], it has been proven that, if $x^*(\cdot)$ is the optimal solution, then there exists an $N = N_\varepsilon$ such that $\|x^{N_\varepsilon}(\cdot) - x^*(\cdot)\| \leq \varepsilon$ with $x^{N_\varepsilon}(t)$ given by,

$$x^{N_\varepsilon}(t) = \sum_{j=0}^{N_\varepsilon} \frac{W(t)}{W(t_j)} \phi_j(t) x_j \tag{21}$$

Although the practice of PS techniques requires that $\varepsilon \geq \varepsilon_m$, the theory allows ε to go to zero in the limit,

$$\lim_{N_\varepsilon \to \infty} x^{N_\varepsilon}(t) = x^*(t) \quad \text{for almost all } t \in [t_0, t_f] \tag{22}$$

That is, an exact (or very high precision) computation of the solution is possible provided the following conditions are met:

1. $W(t) \equiv 1$, $t_j, j = 0, 1, \ldots N_\varepsilon$ are the collection of Gauss-Lobatto points, and the horizon is finite.
2. $W(t) \equiv 1 - t$, $t_j, j = 0, 1, \ldots N_\varepsilon$ are the collection of Gauss-Radau points, and the horizon is (semi-)infinite.

Note that these concepts are similar in spirit to the computation of non-polynomial analytic functions such as e^x or $\ln x$. This is why PS methods are regarded as a joint theoretical-computational approach. Furthermore, under these conditions the PS approach satisfies the Covector Mapping Principle:

Covector Mapping Principle *Let the sequence of function pairs $t \mapsto \{x^N, u^N\}_{N=0}^{\infty}$ converge to a solution of Problem B. Then, there exist multipliers for Problem B^N that map to the coefficients of some interpolating functions that converge to covector functions that solve the dualized version of Problem B.*

Problem B^N in the Covector Mapping Principle is given by,

$$\mathsf{B}^N : \left\{ \begin{array}{lrl} \text{Minimize} & J[\mathbf{x}(\pi^N), \tau_{\text{cmd}}(\pi^N), t_N] & = t_N \\ \text{Subject to} & \dot{\mathbf{x}}^N(t_k) & = \left. \left\{ \begin{array}{l} \frac{1}{2}\mathbf{Q}(\omega)\mathbf{q} \\ \Gamma^{-1} \left[\begin{array}{c} -\omega \times \left(\mathbf{J}\omega + \sum_{i=1}^{4} \mathbf{a}_i I_{\text{w},i} \Omega_{\text{w},i} + \mathbf{a}_i I_{\text{w},i} \mathbf{a}_i^T \omega \right) \\ \mathbf{C}\mathbf{x}_{\text{filt}} + \mathbf{D}\tau_{\text{cmd}} \end{array} \right] \\ \mathbf{A}\mathbf{x}_{\text{filt}} + \mathbf{B}\tau_{\text{cmd}} \end{array} \right\} \right|_{t=t_k} \\ & \mathbf{x}(t_0) & = \left[\mathbf{e}_0 \sin(\frac{\phi_0}{2}), \cos(\frac{\phi_0}{2}), \omega_0, \Omega_0, \mathbf{x}_{\text{filt},0}) \right]^T \\ & \mathbf{x}(t_N) & = \left[\mathbf{e}_f \sin(\frac{\phi_N}{2}), \cos(\frac{\phi_N}{2}), \omega_N, \Omega_N, \mathbf{x}_{\text{filt},N}) \right]^T \\ & ||\mathbf{q}(t_k)|| & = 1 \\ & |\omega_i(t_k)| & \leq \omega_{\max}, \quad i = 1, \ldots, 3 \\ & |\tau_{\text{cmd},i}(t_k)| & \leq \tau_{\text{cmd,max}}, \quad i = 1, \ldots, 4 \\ & |I_{\text{w},i}\Omega_{\text{w},i}(t_k)| & \leq I_{\text{w},i}\Omega_{\max}, \quad i = 1, \ldots, 4 \\ & \tau_L & \leq I_{\text{w},i}\dot{\Omega}_{\text{w},i}(t_k) \leq \tau^U, \quad i = 1, \ldots, 4 \\ & k & = 0, 1, \ldots, N \end{array} \right. \tag{23}$$

where $\pi^N = \{t_0, t_1, \ldots, t_N\}$ is a Gauss-Lobatto grid, $\dot{x}^N(t_k)$ is the derivative of $x^N(t)$ evaluated at t_k

and is obtained quite simply by differentiating (21):

$$\dot{x}^N(t_k) = \sum_{j=0}^{N} \dot{\phi}_j(t_k) x_j \tag{24}$$

Note that once the grid, π^N is selected, the quantity, $\dot{\phi}_j(t_k),\ j,k = 0,\ldots,N$, called the differentiation matrix, is completely determined. That is, it does not depend upon the values of the function.

The Covector Mapping Principle provides the adjoint covector function via the expansion [14],

$$\lambda^{N_\varepsilon}(t) = \sum_{j=0}^{N_\varepsilon} \frac{W^*(t)}{W^*(t_j)} \phi_j(t) \lambda_j \tag{25}$$

where W^* is a dual weight function. The weight functions are of the simplest form when the Legendre-Gauss-Lobatto grid is chosen. That is, $W(t) \equiv W^*(t) \equiv 1$ for the Legendre-Gauss-Lobatto grid.

As a consequence of these fundamental concepts, Pontryagin's Principle can now be applied quite readily to verify and validate the resulting solution. The solution is obtained via a fast spectral algorithm implemented in DIDO [15], an object-oriented MATLAB software package that is agnostic to the details of the PS theory as experienced by the user. Thus, solving Problem B is now raised to the level of a technology wherein flight operations require verification, validation and pre-flight checkouts designed to ensure the success of the mission.

3.4. Pre-Flight Checkout

Pre-flight checkout of solutions to Problem B^N was carried out using a series of standard tests that include continuous-time feasibility and discrete-time optimality checks [15]. The former are carried out by propagating the optimal control trajectory through the system dynamic equations and the latter are accomplished through the automatic application of the Covector Mapping Principle to verify the necessary conditions on the optimality of each solution. Following the analysis of each maneuver from the computational point of view, the ability of the TRACE spacecraft to properly execute each STM was verified against a high-fidelity simulation model of the spacecraft developed at the Naval Postgraduate School. Similar maneuver verification tests were performed independently by flight software specialists at the NASA Goddard Space Flight Center. All of these pre-flight checkout activities were mandatory because shortest-time maneuvers have never been implemented on spacecraft prior to our first experiments on TRACE [11]. After all of the necessary pre-flight checkout activities were successfully completed, the TRACE flight operations team developed the necessary procedures for implementing the maneuvers on orbit. Although STMs are non-eigenaxis maneuvers, the maneuvers were implemented without any modification to the existing eigenaxis ACS. This was done by closely approximating the optimal attitude trajectories as a series of high-frequency, small-angle, eigenaxis rotations compatible with the existing ACS logic.

4. Flight Test Results

This section presents the results of several flight experiments that demonstrate the new approach to maximizing spacecraft imaging capability. The flight tests were carried out using the TRACE spacecraft as a proof-of-concept testbed. Although TRACE is a Sun pointing rather than an Earth pointing satellite, the maneuver scenarios performed onboard TRACE were designed to closely emulate the various types of activities that are relevant to imaging operations on an Earth imaging satellite. In the first test, a shortest-time reorientation maneuver is performed to illustrate the typical improvement in maneuvering performance that can be achieved by implementing STMs in lieu of conventional slews. The results of two additional flight tests are then presented to further demonstrate STM capabilities relevant to the operation of an Earth imaging satellite. The operationally relevant *STAR* maneuver illustrates a sequence of STMs that minimize the time to slew through a sorted set of static imaging points. A second operationally relevant *SCAN* maneuver demonstrates how STMs are utilized to minimize the time to transition between two orthogonal imaging swaths.

4.1. Typical Shortest-Time Maneuver

To experimentally demonstrate the improvement in spacecraft agility that is possible by implementing STMs, a large-angle reorientation maneuver was designed and implemented on TRACE. In the experiment the spacecraft was rotated, in the shortest-time, from an initial attitude quaternion given as $q_o = [0.0, 0.0, 0.43, 0.90]^T$ to the final attitude, $q_f = [-0.31, 0.07, -0.20, 0.93]^T$. An equivalent eigenaxis maneuver was also performed on orbit by rotating the spacecraft through an angle of $\Phi = 80$ degrees around the Euler axis, $\mathbf{e} = [-0.39, 0.30, -0.87]^T$. Some telemetry data pertaining to these two flight tests is given in Fig. 4. An ideal eigenaxis rotation is depicted by a straight line in the projected quaternion space. Fig. 4a clearly shows that for the STM, the plot of q_3 vs. q_2 is far from a straight line. Thus, the instantaneous rotational axis of the STM deviates significantly from the eigenaxis. On the other hand, the flight results for the eigenaxis maneuver show the expected straight line behavior in the quaternion space. Fig. 4a also suggests that the shortest-time maneuver is the space analog of the classic Brachistochrone problem in which the spacecraft executes a longer path than an eigenaxis maneuver but reaches the goal faster.

Fig. 4b shows the time-histories of the cumulative eigenangles for both the shortest-time and eigenaxis maneuvers. The cumulative eigenangle is a measure of the length of the angular path that is traced out by the spacecraft boresight as the spacecraft rotates between the initial and final attitudes. Referring to Fig. 4b, the angular path traced out by the STM is approximately 20 degrees longer than the shortest angular path provided by the eigenaxis rotation. Despite this, the STM could be completed approximately 36 seconds (21%) more quickly than the eigenaxis rotation. This apparent contradiction to intuition is possible because the shortest-time solution finely balances the tradeoff between the available control authority and the spacecraft inertia properties over the entire maneuver. As a consequence, the STM builds body rates around all three spacecraft axes simultaneously as predicted by the cube-shaped spacecraft agilitoid (see Fig. 3b). This enables the spacecraft to traverse the slightly longer shortest-time path more quickly than the eigenaxis rotation.

The peak value of the spacecraft body rate magnitude computed from the available telemetry data was 0.86 deg/sec for the shortest-time maneuver. This value is consistent with the maximum achievable rate of $\sqrt{3}\omega_{\max} = 0.87$ deg/sec, which is obtained when all three body rates are maximized along a diagonal of the agility cube defined by the rate gyro soft-limits, which incorporate a factor of safety. In contrast, for the eigenaxis rotation, it was only possible to maximize the angular rate around the spacecraft z-axis. Thus, the peak value of the body rate magnitude for the eigenaxis maneuver was limited by the much smaller per-axis gyro limit $\omega_{\max} = 0.5$ deg/sec. As a result, the shorter eigenaxis path takes longer to traverse than the path associated with the STM.

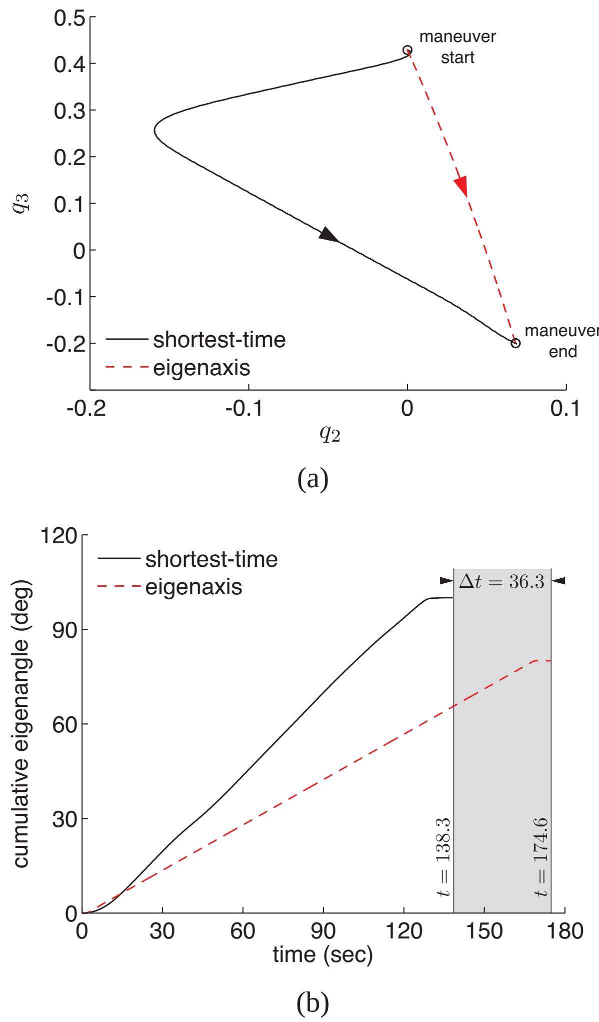

Figure 4. Flight data for shortest-time and eigenaxis maneuvers implemented on TRACE: (a) spacecraft attitude in projected quaternion space; (b) maneuver cumulative eigenangles.

4.2. STAR Maneuver

To demonstrate the merit of shortest-time maneuvering capabilities in more realistic operational scenarios, additional flight test experiments were performed. The first of these operationally relevant flight experiments involved a series of shortest-time maneuvers between a presorted sequence of static imaging points. In this experiment, STMs were utilized to re-point the boresight of the spacecraft towards various Celestial targets as quickly as possible. The objective was to reduce the slew time between each emulated imaging point. This experiment therefore demonstrates how STMs can be used to improve imaging throughput within a given imaging window.

The selected quaternions for the maneuver sequence are the vertices of a five-pointed star. Hence, this maneuver is referred to as the *STAR* maneuver. The five points of the star all constitute potential locations for data collection. Maneuvering between any two points of the star requires the spacecraft to be rotated around a several different eigenaxes. This allows the spacecraft to be exercised over a reasonably large envelope of operation so that a good representation of the overall improvement in maneuvering performance can be obtained from a single flight test. The sequence of desired spacecraft attitude quaternions for the *STAR* maneuver is given in Table 1, along with the yaw-pitch-roll (YPR) Euler angles, relative to the starting quaternion. In order to implement the flight experiment, shortest-time maneuvers were solved between each desired orientation and subsequently executed on the spacecraft. Once coming to rest at each desired orientation, a 30 sec hold period was initiated in order to emulate the image collection activity. Immediately following the hold period, the spacecraft was slewed to the next attitude by following the newly computed shortest-time path. The *STAR* maneuver was also executed as a series of equivalent eigenaxis slews, for performance comparison.

	quaternions				YPR Euler angles (deg)		
maneuver	q_1	q_2	q_3	q_4	$\Delta\phi$	$\Delta\theta$	$\Delta\psi$
$1 \to 2$	0.1302	0.0085	0.0648	0.9893	15.0	0.0	7.5
$2 \to 3$	-0.1302	-0.0085	0.0648	0.9893	-15.0	0.0	7.5
$3 \to 4$	0.0648	-0.0085	-0.1302	0.9893	7.5	0.0	-15.0
$4 \to 5$	0.0000	0.0000	0.1305	0.9914	0.0	0.0	15.0
$5 \to 6$	-0.0648	0.0085	-0.1032	0.9893	-7.5	0.0	-15.0
$6 \to 7$	0.0000	0.0 000	0.0 000	1.0000	0.0	0.0	0.0

Table 1. Sequence of desired spacecraft attitudes for the operationally relevant *STAR* maneuver.

Flight test results for the *STAR* maneuver are shown in Fig. 5. Fig. 5a shows the motion of the imaging boresight (aligned with the spacecraft y-axis) as a projection onto the emulated imaging plane. Each trace was reconstructed from telemetry data captured during the flight test experiment. Time-histories of the yaw-pitch-roll Euler angles are shown in Fig. 5b, for reference. The telemetry data clearly shows that the motion of the imaging boresight deviates from the eigenaxis for each shortest-time maneuver. Moreover, the spacecraft is observed to follow a slightly different shortest-time path as it rotates between each desired orientation. This is because the shapes of the shortest-time maneuver trajectories are dependent upon the maneuver boundary conditions in relation to the spacecraft agilitoid (see Fig. 3). Flight test results for the eigenaxis *STAR* maneuver are given in Fig. 6. As expected, Fig. 6a shows that the spacecraft slews along the shortest circular arcs (straight line paths) between each of the desired orientations. Inspection of the time-histories of the Euler angles for the eigenaxis maneuver (Fig. 6b) confirms that the eigenaxis *STAR* maneuver takes longer to complete than the shortest-time *STAR* maneuver. The overall reduction in slew time for the entire *STAR* maneuver is approximately 10%. The range of individual slew time improvements varied between 2% and 24% depending on the initial and final attitude angles and their relation to the spacecraft agilitoid.

The 10% overall improvement in slew performance may seem modest, but it is important to note that the TRACE spacecraft was never intended to perform large reorientation maneuvers, let alone shortest-time maneuvers. Thus, the agility capability of the spacecraft was severely restricted by the relatively small saturation limit of the onboard gyros. The improvement in slew performance can, in fact, be much larger when STMs are developed for spacecraft specifically designed for imaging operations. Our recent ground experiments on a CMG-actuated spacecraft simulator at Honeywell have indicated that it is possible to decrease slew times by up to 50% through the implementation of STMs [28]. As a consequence, the capability of an imaging spacecraft can be significantly improved simply by changing how the spacecraft is maneuvered from point to point. Moreover, no change in the actuator hardware is necessary to realize the performance improvement.

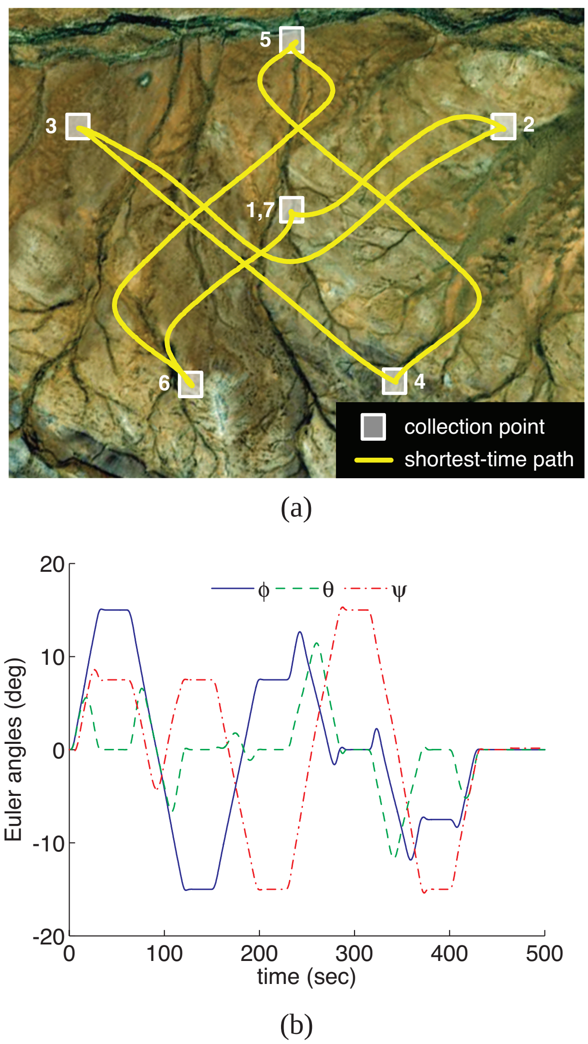

Figure 5. Flight results for the shortest-time *STAR* maneuver: (a) projection of boresight motion in the imaging plane; (b) relative yaw-pitch-roll Euler angles.

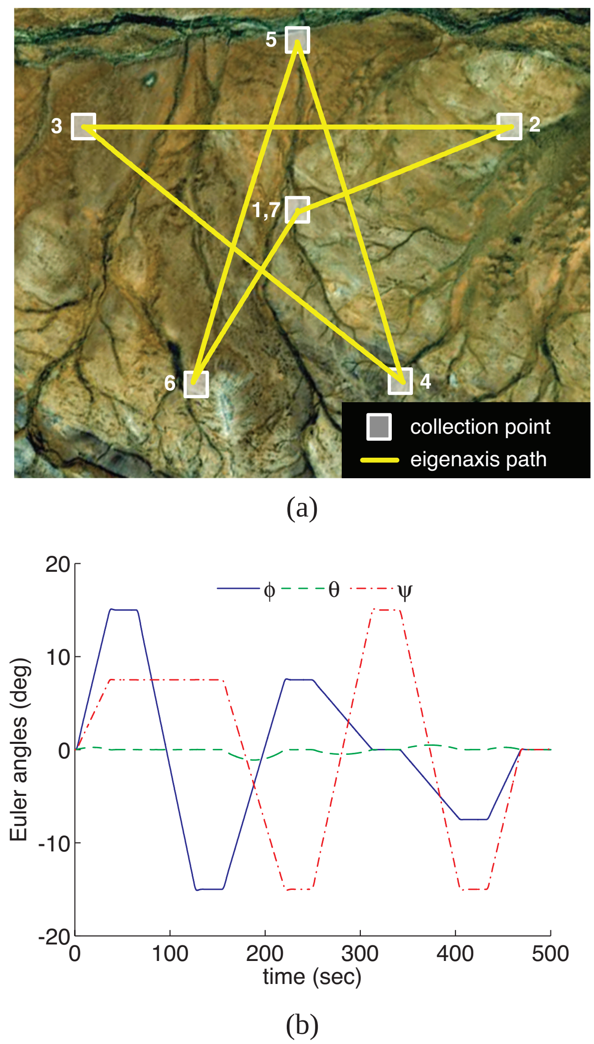

Figure 6. Flight results for the eigenaxis *STAR* maneuver: (a) projection of boresight motion in the imaging plane; (b) relative yaw-pitch-roll Euler angles.

4.3. Orthogonal SCAN Maneuver

The orthogonal *SCAN* maneuver represents another operational scenario relevant to the operation of an imaging spacecraft. This maneuver emulates an imaging process in which the satellite sensor collects data along a swath or scan-line. The objective in this case is to slew as quickly as possible between transition points which mark the initiation and completion of each scanning operation. Two orthogonal collection swaths, one parallel to and one perpendicular to the assumed ground track, are included as part of the experiment in order to stress the spacecraft attitude control system and demonstrate an ability to implement STMs having a variety of different non-zero boundary conditions. This experiment illustrates how STMs can be utilized to quickly transition a spacecraft between point collection and scanning operations.

Telemetry results for the *SCAN* maneuver test are shown in Fig. 7. Fig. 7a, shows the motion trace of the imaging boresight. Referring to Fig. 7a, the first STM starts from the home orientation and ends when the spacecraft reaches a specified attitude at location *A*. At attitude *A*, non-zero attitude rates are maintained to perform the scanning maneuver (see Fig. 7b). To transition from the first scan region to the second scan region (lying in a direction orthogonal to the first), a second STM is performed between points *B* and *C*. Once the desired spacecraft orientation is reached as point *C*, a second scan maneuver is performed by maintaining specified non-zero attitude rates between attitudes *C* and *D*. The *SCAN* maneuver is completed by a final STM between attitude *D* and a static imaging point (also located at the home position). An interesting feature of the *SCAN* maneuver is the nonintuitive path traced out by the spacecraft boresight as the vehicle transitions between the two scan regions. In particular, the spacecraft first moves away from and then overshoots point *C* before initiating the second scan. This surprising and unexpected result emphasizes how the proposed optimal control technique can be leveraged to enhance the imaging capability of Earth imaging spacecraft beyond what is possible using conventional approaches for maneuver design.

5. Conclusion

This paper presented flight test results from a shortest-time maneuvering experiment carried out on the NASA space telescope TRACE. Shortest-time maneuvers (STM)s are spacecraft slew maneuvers, based on optimal control theory, that have the potential to revolutionize the operation of imaging spacecraft by enabling spacecraft to be reoriented more quickly than conventional maneuvers. In order to design each STM, a detailed model of the TRACE spacecraft and its reaction wheel actuation system was first developed. The spacecraft model contained sufficient fidelity to ensure that the designed maneuvers could be reliably executed by the orbiting spacecraft. The spacecraft dynamic model was then embedded, along with the appropriate constraints, in an optimal control problem formulation that was subsequently solved using the Legendre pseudospectral method implemented in the object-oriented software package DIDO. The flight test results clearly show that implementing STMs, in lieu of conventional maneuvers, can significantly improve the agility of the spacecraft. Moreover, the improved performance can be realized simply by changing the commanded maneuver trajectories and hence does not require the existing spacecraft attitude control system to be otherwise modified. The successful flight demonstration of several operationally relevant maneuvers, each designed to emulate scenarios encountered as part of the daily operation of an Earth imaging satellite, illustrate that it is now possible to insert the revolutionary approach for maximizing spacecraft imaging capability into normal mission operations. This technology is currently being transitioned to industry.

6. Acknowledgments

The authors wish to acknowledge K. Lebsock (NASA Engineering & Safety Center), R. Chen (K & D Research) and T. Correll (GSFC) for their help in explaining the intricacies of the TRACE spacecraft and its attitude control system as well as the tireless assistance of O. Cuevas (GSFC), M. Baugh (GSFC), S. Snell (Computer Sciences Corporation), D. Bradley (Honeywell Technology Solutions), and the outstanding efforts of the flight operations team in the Multi-Mission MOC at the NASA Goddard Space Flight Center who were instrumental in coordinating the flight experiments.

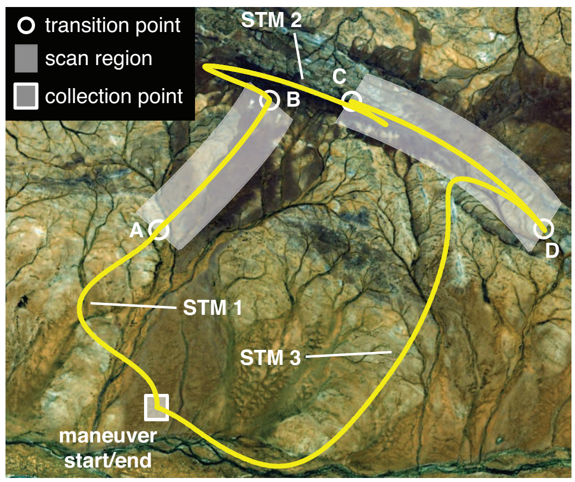

(a)

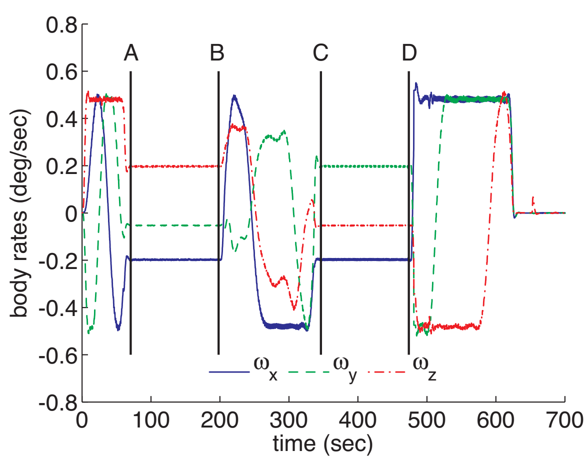

(b)

Figure 7. Flight results for the shortest-time orthogonal *SCAN* maneuver: (a) projection of boresight motion in the imaging plane; (b) spacecraft body rates.

7. References

[1] Cordeau, J.-F. and Laporte, G. “Maximizing the value of an earth observation satellite orbit.” Journal of the Operational Research Society, Vol. 56, pp. 962–968, 2005.

[2] Mansour, M. A. A. and Dessouky, M. M. “A genetic algorithm approach for solving the daily photography selection problem of the SPOT5 satellite.” Computers and Industrial Engineering, Vol. 58, No. 3, pp. 509–520, 2010.

[3] Bayir, I. “IKONOS collection capability with the direct tasking from a regional operation center.” “Proceedings of the 2003 International Conference on Recent Advances in Space Technologies,” pp. 30–33. Istanbul, Turkey, 2003.

[4] Bilimoria, K. D. and Wie, B. “Time-optimal three-axis reorientation of rigid spacecraft.” Journal of Guidance, Control and Dynamics, Vol. 16, No. 3, pp. 446–452, 1993.

[5] Scrivener, S. L. and Thompson, R. C. “Survey of time-optimal attitude maneuvers.” Journal of Guidance, Control and Dynamics, Vol. 17, No. 2, pp. 225–233, 1994.

[6] Shen, H. and Tsiotras, P. “Time-optimal control of axisymmetric rigid spacecraft using two controls.” Journal of Guidance, Control and Dynamics, Vol. 22, No. 5, pp. 682–694, 1999.

[7] Proulx, R. and Ross, I. M. “Time-optimal reorientation of asymmetric rigid bodies.” Advances in the Astronautical Sciences, Vol. 109, pp. 1207–1227, 2001.

[8] Modgalya, M. and Bhat, S. P. “Time-optimal attitude reorientation at constant angular velocity magnitude with bounded angular acceleration.” “Proceedings of the 2006 IEEE Conference on Decision and Control,” pp. 223–228. San Diego, CA, 2006.

[9] Lee, T., Leok, M., and McClamroch, N. H. “Time optimal attitude control for a rigid body.” “Proceedings of the 2008 American Control Conference,” pp. 5210–5215. Seattle, WA, 2008.

[10] Fleming, A., Sekhavat, P., and Ross, I. M. “Minimum-time reorientation of a rigid body.” Journal of Guidance, Control and Dynamics, Vol. 33, No. 1, pp. 160–170, 2010.

[11] Karpenko, M., Bhatt, S., Bedrossian, N., Fleming, A., and Ross, I. M. “First flight results on time-optimal spacecraft slews.” Journal of Guidance, Control and Dynamics, Vol. 35, No. 2, pp. 367–376, 2012.

[12] Fahroo, F. and Ross, I. M. “Advances in pseudospectral methods for optimal control.” “AIAA Guidance, Navigation, and Control Conference,” AIAA Paper 2008-7309. 2008.

[13] Gong, Q., Fahroo, F., and Ross, I. M. “A spectral algorithm for pseudospectral methods in optimal control.” Journal of Guidance, Control and Dynamics, Vol. 31, No. 3, pp. 460–471, 2008.

[14] Ross, I. M. and Karpenko, M. “A review of pseudospectral optimal control: from theory to flight.” Annual Reviews in Control, to appear.

[15] Ross, I. M. "A beginner's guide to DIDO: A MATLAB application package for solving optimal control problems." Tech. Rep. TR-711, Elissar Global, Carmel, CA, November 2007.

[16] Bedrossian, N., Bhatt, S., Kang, W., and Ross, I. M. "Zero-propellant maneuver guidance." IEEE Control Systems Magazine, pp. 53–73, October 2009.

[17] "TRACE home page (2011, Sept. 14)." http://sunland.gsfc.nasa.gov/smex/trace/.

[18] Sidi, M. J. Spacecraft Dynamics and Control. Cambridge University Press, New York, 1997.

[19] Zimbelman, D., Wilmot, J., and Evangelista, S. "The attitude control system design for the transition region and coronal explorer mission." "Proceedings of the 10th Annual AIAA/USU Conference on Small Satellites," Logan, UT, 1996.

[20] Ross, I. M. A primer on Pontryagin's principle in optimal control. Collegiate Publishers, San Francisco, 2009.

[21] Williams, P. "Jacobi pseudospectral method for solving optimal control problems." Journal of Guidance, Control and Dynamics, Vol. 27, No. 2, pp. 293–297, 2004.

[22] Kang, W. "Rate of convergence for the Legendre pseudospectral optimal control of feedback linearizable systems." Journal of Control Theory and Applications, Vol. 8, No. 4, pp. 391–405, 2010.

[23] Kang, W., Ross, I. M., and Gong, Q. Analysis and Design of Nonlinear Control Systems, chap. Pseudospectral optimal control and its convergence theorems, pp. 109–126. Springer-Verlag, Berlin Heidelberg, 2008.

[24] Fahroo, F. and Ross, I. M. "Convergence of the costates does not imply convergence of the control." Journal of Guidance, Control and Dynamics, Vol. 31, No. 5, pp. 1492–1497, 2008.

[25] Kang, W., Gong, Q., and Ross, I. M. "On the convergence of nonlinear optimal control using pseudospectral methods for feedback linearizable systems." International Journal of Robust and Nonlinear Control, Vol. 17, No. 14, pp. 1251–1277, 2007.

[26] Gong, Q., Kang, W., and Ross, I. M. "A pseudospectral method for the optimal control of constrained feedback linearizable systems." IEEE Transactions on Automatic Control, Vol. 51, No. 7, pp. 1115–1129, 2006.

[27] Ross, I. M. and Fahroo, F. Lecture Notes in Control and Information Sciences, Vol. 295, chap. Legendre pseudospectral approximations of optimal control problems, pp. 327–342. Springer-Verlag, New York, 2003.

[28] Karpenko, M., Bhatt, S., and Hamilton, B. "Application of pseudospectral optimal control for shortest-time spacecraft attitude maneuvers." Presented at the IEEE Conference on Decision and Control, Workshop on Guidance, Navigation and Control Applications in the Aerospace Industry, 2012 [PowerPoint slides].